

T-Cell Derived Lipocalin-2 Upregulates TNF- $\alpha$  in Optic Nerve Head Astrocytes

Nemahun H. Vincent

A Thesis in the Field of Biology  
for the Degree of Master of Liberal Arts in Extension Studies

Harvard University

March 2020



## Abstract

The purpose of this study was to investigate lipocalin-2 (Lcn2) as a potential reactive astrocyte marker in the glaucomatous optic nerve. Glaucoma is a disease of the optic nerve that results in irreversible vision loss secondary to retinal ganglion cell damage and astrocyte reactivity in response to glaucomatous injury. Due to the role of Lcn2 in reactive astrocytes of glaucomatous optic nerves being poorly elucidated, we studied Lcn2 in the setting of optic nerve crush (ONC), DBA/2J, and microbead injection (ocular hypertension) models. In situ hybridization and immunohistochemistry (IHC) were used to detect and localize Lcn2 in tissue samples. Quantification was performed using qPCR. We found that Lcn2 expression is upregulated in the ONC and DBA/2J models, but not in the microbead injection model. IHC revealed Lcn2<sup>+</sup> cells starting 4 h following ONC. However, in contrast to what was expected, these cells were not astrocytes or microglia. Instead, the co-labeling of Lcn2<sup>+</sup> cells with CD3 indicates a T-cell population. qPCR screening of ONH astrocytes cultured in Lcn2 revealed that neither the neurotoxic A1 nor neuroprotective A2 reactive astrocyte phenotype was acquired. Instead, Lcn2 differentially upregulated the inflammatory marker TNF- $\alpha$  in astrocytes, thus demonstrating that Lcn2 is not a marker for reactive astrocytes. These findings propose a link between Lcn2 and TNF- $\alpha$  that may be key in decreasing ON inflammatory degeneration.

## Acknowledgments

I am deeply grateful to my thesis director, Dr. Tatjana Jakobs. She dependably and patiently offered advice, support, as well as frequent encouragement that I found to be indispensable. The countless time she spent counseling and guiding me throughout this process was very much appreciated. Many thanks extended to Dr. James Morris for his kindness and assistance during the process of getting my project to a completed state, and Dr. Meredith Gregory-Ksander for critically reading this thesis. I would also like to thank Dr. Daniel Sun, Dr. Ying Zhu, and Dr. Song Li for their help throughout this project.

## Table of Contents

Acknowledgments.....	iv
List of Tables .....	vii
List of Figures .....	viii
Chapter I Introduction.....	1
Glaucoma Background.....	1
Current Glaucoma Treatments .....	7
Animal Models of Glaucoma.....	8
LCN2 Background.....	10
Neuroinflammation Background .....	12
Chapter II. Materials and Methods .....	15
<i>Animal husbandry</i> .....	15
<i>Retro-orbital optic nerve crush (ONC)</i> .....	15
<i>Microbead occlusion model of ocular hypertension (OHT)</i> .....	16
<i>Measurement of intraocular pressure (IOP)</i> .....	17
<i>Tissue collection and processing</i> .....	18
<i>Immunohistochemistry (IHC)</i> .....	18
<i>Image acquisition and analysis</i> .....	19
<i>In situ hybridization (ISH)</i> .....	19
<i>Astrocyte Collection, RNA extraction, and cDNA synthesis</i> .....	19
<i>Quantitative PCR (qPCR)</i> .....	20

<i>Statistical Analysis</i> .....	21
Chapter III Results .....	22
Lcn2 in the Crushed Optic Nerve .....	22
Immunohistochemistry .....	22
<i>In situ</i> hybridization .....	24
Microbead Occlusion Model of Ocular Hypertension.....	25
Lcn2 in DBA/2J .....	27
qPCR Analysis of Lcn2 Regulation in Cultured Astrocytes.....	29
Chapter IV Discussion .....	31
Appendix 1. qPCR Primer Sequences .....	36
References.....	39

## List of Tables

Table 1. List of qPCR Primer Sequences used to screen for Lcn2 regulation in astrocytes isolated from C57BL/6 pups.....	38
--	----

## List of Figures

Figure 1. Schematic illustrating the TM outflow pathway. ....	3
Figure 2. Cross section of the globe; zoom view of the retina. ....	4
Figure 3. RGC axon layouts.....	5
Figure 5. <i>In situ</i> hybridization staining of Lcn2 in the optic nerve.....	24
Figure 6. Ocular hypertension induced via microbead injection. ....	26
Figure 7. Immunohistochemistry in the ON following microbead injection.....	27
Figure 8. Immunohistochemistry of optic nerves from DBA/2J mice.....	28
Figure 9. qPCR for markers of astrocyte reactivity and neuroinflammation.....	30

## Chapter I

### Introduction

#### Glaucoma Background

Glaucoma is a multifactorial disease that is one of the leading causes of irreversible vision loss worldwide (Tham et al., 2014). Due to the complex nature of the disease, a cure remains elusive (Bouhenni, Dunmire, Sewell, & Edward, 2012). Nearly 50% of patients are unaware that they have decreased peripheral vision as glaucoma is largely asymptomatic during the early stages of the disease (Quigley, 2011). There are a reported 60 million individuals worldwide that are afflicted, with 8.4 million with bilateral blindness (Quigley, 2011). It is predicted that the number of individuals with glaucoma worldwide will grow to 111.8 million by 2040, and predominantly in Asian and African populations (Tham et al., 2014). There are two major variants of glaucoma: open-angle and angle-closure (narrow-angle) glaucoma (Quigley, 2011). Primary open-angle glaucoma (POAG) is the most prevalent variant in the United States (Distelhorst & Hughes, 2003; Mantravadi & Vadhar, 2015).

Glaucoma is characterized as an optic neuropathy that presents with optic nerve (ON) damage and visual field loss that can be induced by increased intraocular pressure (IOP) and advanced age, which are among the major risk factors (Krizaj, 1995; Quigley, 2011). Other risk factors for developing POAG include trauma to the eye, uveitis, steroid therapy, strong first-degree family history of glaucoma, thin central corneal thickness, black race, and epigenetics (Distelhorst & Hughes, 2003; Mantravadi & Vadhar, 2015).

Because age is a risk factor for glaucoma, it is expected that incidence rates will increase over time as lifespans are expanding (Mantravadi & Vadhar, 2015).

Though a risk factor, elevated IOP is not a defining feature of glaucoma, as an individual can have high ocular pressure yet no damage. As such, IOP-associated factors such as blood flow and biomechanical stress exerted upon the sclera and optic nerve head are considered to play a role in glaucoma pathogenesis (Quigley, 2011).

It is likely that the driving force behind elevated IOP is impaired outflow of aqueous humor via the trabecular meshwork (TM), a significant component of the outflow mechanism (Mantravadi & Vadhar, 2015). The TM can be found in the angle of the eye, an interface formed between the cornea and iris (Mantravadi & Vadhar, 2015).

Aqueous humor is continually produced by the epithelial layers of the ciliary body and secreted into the posterior chamber. The normal outflow mechanism involves passage of aqueous humor from the posterior chamber through the pupil into the anterior chamber (Figure 1). The fluid is drained from the eye via the TM or the less conventional uveoscleral pathway. However, the latter pathway is not involved in IOP generation and maintenance (Mantravadi & Vadhar, 2015).

The trabecular outflow pathway involves passage of aqueous humor through the TM, juxtacanalicular tissue, Schlemm's canal endothelium, and then into the lumen of Schlemm's canal. The fluid is eventually drained into the episcleral veins, which are connected to Schlemm's canal via collector channels (Braunger, Fuchshofer, & Tamm, 2015).

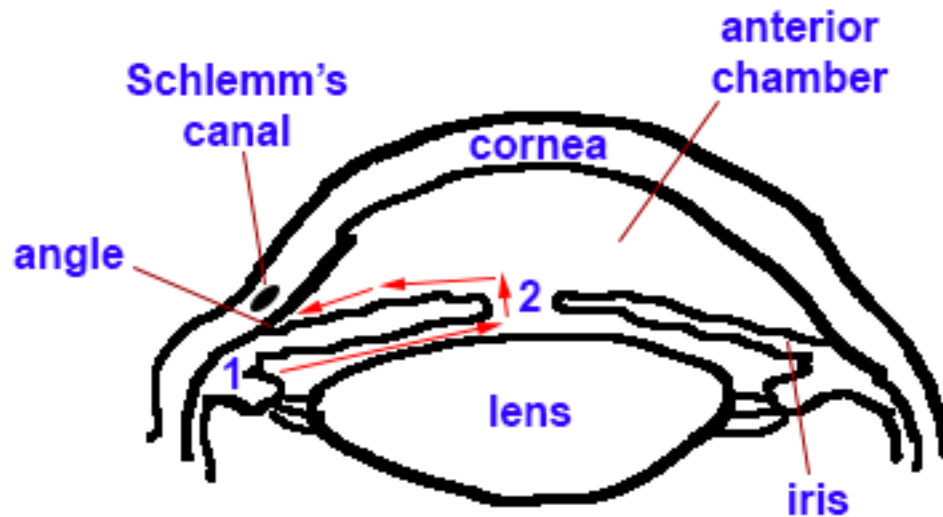


Figure 1. Schematic illustrating the TM outflow pathway.

*The aqueous humor is produced by the ciliary body (1), then passes from the posterior chamber through the pupil (2) into the anterior chamber. The fluid is drained from the eye via the TM and exits through Schlemm's canal located in the drainage angle.*

Under standard conditions, visual outputs are transmitted from the retina to the brain via action potentials conducted by the retinal ganglion cell (RGC) axons which form the optic nerve, chiasm, and tract [Figure 2] (Crish, Sappington, Inman, Horner, & Calkins, 2010). The superior colliculus is the primary location of RGC projection in the rodent brain, while RGCs mainly project to the lateral geniculate nucleus (LGN) in humans (Crish et al., 2010; Sappington, Carlson, Crish, & Calkins, 2010). Of note, RGCs are the only retinal cells that send projections (axons) to the brain.

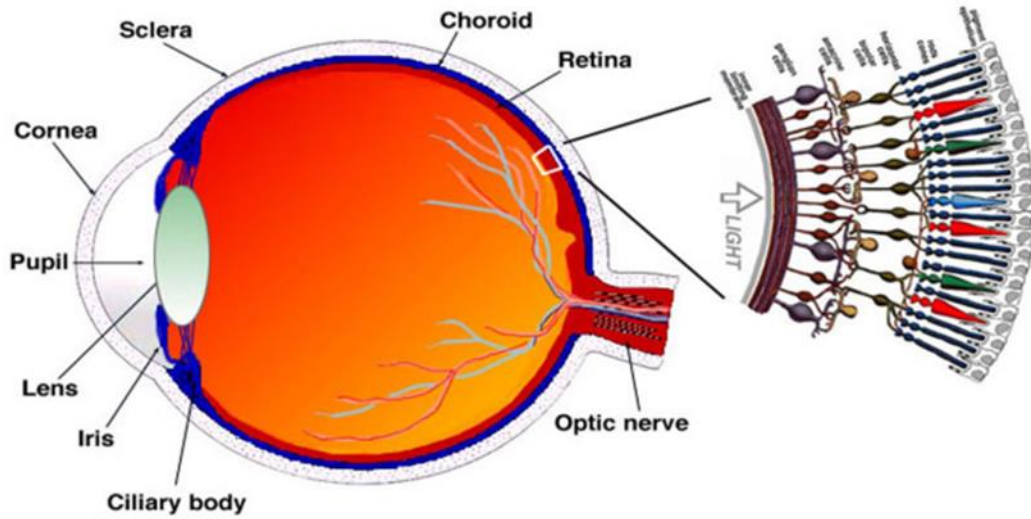


Figure 2. Cross section of the globe; zoom view of the retina.

*Visual inputs are received and projected onto the retina via the lens. The resultant output is transmitted to the brain via RGC axons that form the optic nerve (Kolb, 2011).*

Increased IOP exerts a mechanical force upon the optic nerve fibers at the lamina cribrosa [LC]). The LC is a specialized, porous structure through which RGC axons exit the eye to form the optic nerve. Axons originating from the peripheral retina pass through the peripheral region of the LC, while central retina axons pass through the center. In primates, the LC is comprised of collagen and elastin beams that are lined with fibroblasts, astrocytes, microglia, and a vascular supply. It has been noted that elevated IOPs stiffen the ONH, but it is unclear if a stiffened LC can better withstand mechanical strain (Krizaj, 1995).

Mechanical force has been noted to promote RGC loss, neural rim thinning, and ON cup enlargement (Distelhorst & Hughes, 2003; Mantravadi & Vadhar, 2015). Functional and molecular changes in microglia and astrocytes can also be triggered by mechanical stress (Krizaj, 1995).

Glaucomatous optic neuropathy involves optic disc and LC damage and remodeling that cause vision loss. RGC axon loss results in LC thinning that contributes to excavation of the central disc (Krizaj, 1995). It is important to note that mice do not have an LC or macula (Bouhenni et al., 2012). Instead, rodent RGC axons are structurally and metabolically supported by an analogous structure (the glial lamina) composed of astrocytes (Krizaj, 1995; Sun, Lye-Barthel, Masland, & Jakobs, 2010). The lack of a macula is a limitation of this animal model as it impacts the arrangement of RGC axons in the mouse retina. In humans, RGC axons circumvent the macula [Figure 3] (Kolb, 2011). However, the absence of an LC in mice does not preclude presentation of glaucoma in this species, as glaucomatous optic neuropathy can also be the result of poor blood flow secondary to elevated IOP, increased blood viscosity, or increased flow resistance (Flammer et al., 2002).

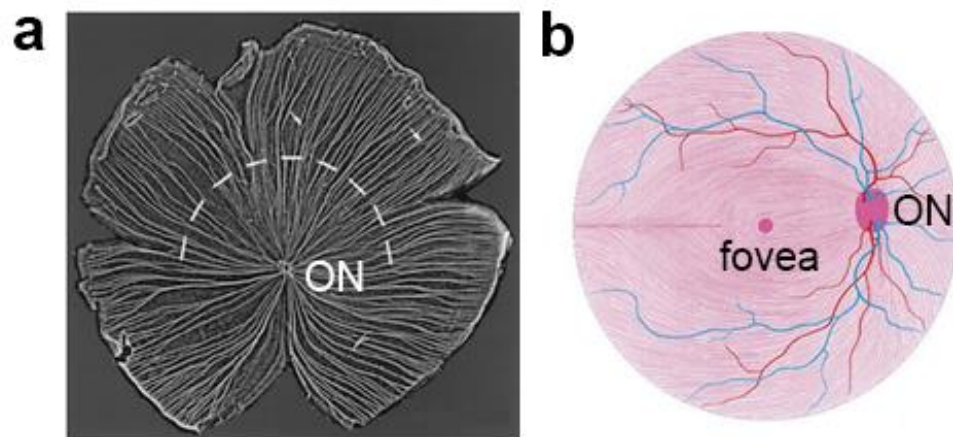


Figure 3. RGC axon layouts.

*The RGC axon layouts in mouse (a, Leppert et al., 1999) and human (b, Kolb, 2011) retinas differ, as the axons bypass the macula (the center of this region is the fovea).*

As the disease course progresses, vision loss in mouse models of glaucoma follows a sectorized pattern and extends to the central retina, which is rich in RGCs (Crish et al., 2010). In humans, visual field defects present as scotomas, or blind spots adjacent to the macula. However, the mechanisms involved in RGC degeneration are not well understood.

As mentioned prior, glaucoma is a largely asymptomatic disease in early glaucoma. Patients can possibly note a gradual loss of peripheral vision after losing greater than 40 percent of ON fibers (Distelhorst & Hughes, 2003). While elevated IOP is a risk factor for glaucoma, approximately two thirds of patients with elevated IOP do not develop ON cupping or visual field loss. These patients are diagnosed as glaucoma suspects. There are also patients that have glaucomatous ON damage despite normal IOP readings. This is classified as normal-pressure glaucoma. As such, early diagnosis is challenging.

Diagnostic findings, such as a progressive increase in cup-to-disc ratio are indicative of advancing ON death and uncontrolled glaucoma (Distelhorst & Hughes, 2003; Quigley, 2011). Enlarged optic nerves are defined as having a cup-to-disc ratio greater than 0.5. Visual field screening and direct ophthalmoscopy are used to confirm a diagnosis of OAG. Field loss becomes more extensive with advancement of glaucomatous damage (Distelhorst & Hughes, 2003).

Presently, the only modifiable OAG risk factor is IOP. Management options include IOP-lowering eye drops, laser treatment, or incisional surgery. However, the aim of glaucoma therapy is vision preservation as monitored by visual field testing, not lowering of IOP. The initial treatment option is topical therapy. There are several classes

of eye drops that can decrease IOP by increasing aqueous outflow or decreasing aqueous production. The first group includes prostaglandin analogs and parasympathomimetics. The latter group includes beta-blockers, carbonic anhydrase inhibitors, and alpha agonists. If monotherapy proves unsuccessful, combination therapy can be considered (Distelhorst & Hughes, 2003; Quigley, 2011).

When eye drops prove ineffective due to patient noncompliance or intolerance, inadequate IOP-lowering effect, or there is progressive ON damage despite low IOP, surgical management is considered. Laser trabeculoplasty is typically a first-line option before considering an incisional procedure such as trabeculectomy. Trabeculectomy is considered in cases where topical and laser treatment has failed to adequately manage the disease course (Quigley, 2011).

### Current Glaucoma Treatments

There are additional topical therapies that have been recently approved by the FDA (e.g. Rhopressa, Vyzulta, Rocklatan). These drugs employ alternative mechanisms of action compared to established drugs, thus providing other options for patients who have maxed out topical therapies due to allergies or drug intolerance. However, side effects may potentially decrease patient compliance, thus suggesting that these drugs will likely be adjuncts to pre-existing therapies (Schehlein & Robin, 2019).

Microinvasive glaucoma surgery (MIGS) is relatively recent development that holds promise. This surgery technique employs microstents such as CyPass, XEN gel, or iStent to lower IOP. However, the CyPass was recently withdrawn from the market for further investigation. Despite clinicians having several treatment options at their disposal, poor patient compliance can limit IOP-lowering efforts, while surgery is not always

effective. Moreover, glaucoma progression can occur despite sufficient IOP reduction with topical IOP-lowering treatments (Kersey, Clement, Bloom, & Cordeiro, 2013). These barriers to successful glaucoma management are indicative of a need for alternative therapies and a clearer understanding of the disease course.

Given the neurodegenerative nature of glaucoma as noted by RGC apoptosis and ON damage, examination of the neurological components of this disease is of interest. In animal models, there are some neuroprotective therapies being studied. However, these have not yet reached the clinical trial stage. Exploration of the potential role of STAT3 upregulation in retinal ganglion cell (RGC) axon protection has been investigated, as has the potential benefit of soluble Fas ligand injection in preventing RGC death (Krishnan et al., 2016; Sun, Moore, & Jakobs, 2017).

### Animal Models of Glaucoma

There are several animal models available to deepen understanding of the underlying mechanisms involved in glaucoma development (Bouhenni et al., 2012). These include rabbit, dog, monkey, rodent, and other species (Bouhenni et al., 2012). Benefits of mouse models include low cost, ease of housing and handling, and conservation between mouse and human genomes (Bouhenni et al., 2012). Other benefits are the ability to genetically modify mice via alteration of the genome, flexibility in animal breeding, and adequate reproduction of certain components of glaucoma. However, no single glaucoma model can capture the complexity of this disease. As such, several animal models were used to study the multiple facets of glaucoma. These comprised of the microbead occlusion model, DBA/2J, and optic nerve crush (ONC).

The microbead occlusion model induces IOP elevation via injection of inert polystyrene and magnetic beads into the anterior chamber (AC) of the eye. The beads initially follow the flow pattern of the aqueous humor. IOP elevation is induced due to the microbeads becoming lodged in the TM, thus impeding aqueous outflow (Sappington et al., 2010). Another model with elements of IOP elevation is DBA/2J. In this inherited glaucoma model, IOP elevation is secondary to iris pigment dispersion into the drainage structures of the eye (Anderson et al., 2002; Bouhenni et al., 2012). The phenotypes of DBA mice are the product of mutations in the *Gpnbm* (pigment dispersion) and *Tyrp1* (iris stromal atrophy) genes (Anderson et al., 2002). The DBA model replicates aspects of the human disease due to retinal, ON, and IOP changes that are variable, age-related, and progressive properties that may occur unilaterally or bilaterally (Bouhenni et al., 2012; Libby et al., 2005). The gene mutations that are responsible for the iris disease also induce an iris-targeting inflammatory response (Libby et al., 2005).

The final model that was used, ON crush, also has an inflammatory component that is secondary to the physical insult imparted upon the ON. Reactive gliosis is induced by ONC, which results in differential expression of ONH genes involved in inflammation and immunity. DNA microarray analysis revealed robust upregulation of lipocalin-2 (*Lcn2*) and other genes immediately after crush, with attenuated expression over time (Qu & Jakobs, 2013). This observation reflected the previously reported findings of *Lcn2* upregulation in several models of ON damage: Howell et al. (2011) studied the ONH of DBA/2J mice while Zamanian et al. (2012) used purified astrocytes isolated from MCAO & LPS-treated brains. Though ONC does not reflect the progressive and chronic nature of glaucoma-induced damage, it does promote robust astrocyte reactivity. Reactive

astrocytes undergo several morphological changes that are likely representative of changes noted in glaucoma (Sun et al., 2010). As a potential reactive astrocyte marker, the role of Lcn2 in glaucoma pathogenesis is of interest.

### LCN2 Background

Neutrophil-gelatinase-associated lipocalin, also known as lipocalin-2, is a 25-kDa secreted glycoprotein that belongs to the lipocalin superfamily (Abella et al., 2015; Song & Kim, 2018). LCN2 is a protein that was first identified in a search for oncogenes and is a member of a family of molecules that can bind prostaglandins, retinols, and pheromones as well as transport lipophilic small molecules. The ligand for LCN2 is a catecholate-type siderophore, a small molecule used by bacteria to search for soluble ferric iron (C. Li & Chan, 2011). LCN2 is involved in innate immunity via iron sequestration by its siderophore. This results in decreased bacterial growth (Flo et al., 2004). Mammalian binding targets have also been identified, including solute carrier family 22 member 17 (SLC22A17) and megalin (Bi et al., 2013; C. Li & Chan, 2011).

LCN2 has been implicated in several other biological processes as well as innate immunity, including cell migration, apoptosis, and differentiation (Abella et al., 2015; Song & Kim, 2018). Many organs can produce LCN2 in response to injury, including the kidney, liver, and brain (Abella et al., 2015). LCN2 receptors have been found in neurons, microglia, and astrocytes (Song & Kim, 2018). When released by glial cells, LCN2 is involved in neuronal cell death, reactive astrocytosis, neuroinflammation, and serves as a chemokine inducer in the central nervous system (CNS) (Abella et al., 2015; Song & Kim, 2018). However, the role of LCN2 in the CNS is poorly understood.

Several groups have noted that LCN2 upregulation is neurotoxic and can induce neuroinflammation. In animal models of experimental autoimmune encephalomyelitis (EAE) and ischemic stroke, LCN2 gene knockout proved neuroprotective (Kim et al., 2016). Chun et al. (2015) noted increased LCN2 expression in optic nerve tissue sections of mice with induced experimental autoimmune optic neuritis (EAON) versus wild-type. Co-localization of LCN2 expression with cells positive for an astrocyte-specific marker, GFAP, indicates that reactive astrocytes within the optic nerve can induce LCN2 expression. Thus, LCN2 derived from astrocytes may be crucial to recruiting peripheral inflammatory and immune cells into the optic nerve (Chun et al., 2015). Bi et al. (2013) observed the selective neurotoxicity of LCN2 after release by astrocytes activated in the setting of neurodegenerative diseases.

However, Berard et al. (2012) noted a deleterious effect of LCN2 deficiency in EAE (Kim et al., 2016). In their study, Xing et al. (2014) measured LCN2 in brain samples from rats in which cerebral ischemia had been induced in a human stroke patient. It was found that neuronal expression of LCN2 was increased in these tissue samples, and that LCN2 is released by damaged neurons as a means of soliciting help from microglia and astrocytes to potentially induce healing or initiate a prorecovery state (Xing et al., 2014).

At the optic nerve head, astrocytes surround ganglion cell axons (Sun, Lye-Barthel, Masland, & Jakobs, 2009; Wang, Seifert, & Jakobs, 2017). It has been observed that these astrocytes become reactive in response to glaucoma or traumatic injury (Wang et al., 2017). As such, it appears that astrocytes are involved in glaucoma pathogenesis. However, it is not known if LCN2 is released by astrocytes in glaucomatous optic nerves

nor if LCN2 is neurotoxic or neuroprotective in this context. In various models with an inflammatory component (DBA/2J mice, optic nerve crush, MCAO), LCN2 is one of the most highly upregulated genes.

### Neuroinflammation Background

The blood-brain-barrier (BBB) protects the central nervous system (CNS), which includes the eye and optic nerve, from peripheral immune and inflammatory responses, of which there are acute and chronic variants. The acute inflammatory response occurs upon injury initiation. Acute responses are temporary and neutralize threats to the CNS by mitigating cellular damage. Contrarily, a chronic inflammatory response can be deleterious and result in neuronal damage as well as neurodegeneration due to prolonged buildup of neurotoxic proinflammatory mediators. Acute inflammatory responses become chronic when inflammation resolution and repair do not occur within a short time frame (Bazan, Halabi, Ertel, & Petasis, 2012).

Neuroinflammatory responses noted in glaucoma demonstrate classical inflammatory CNS responses to injury, disease, or infection (Bazan et al., 2012; Soto & Howell, 2014). Neuroinflammation is typically defined as chronic inflammation of the CNS, and is a response that involves all CNS cells. Due to limited interaction between the CNS and the systemic immune system, CNS immune responses are typically mediated by a limited number of cell types, namely glial cells. Astrocytes are the most abundant type of CNS cell and hold several functions, including BBB and homeostasis maintenance. Microglia are the resident macrophages and a major immune mediator in the CNS.

Glial cells are activated by proinflammatory stimulants, thus triggering the production of cytokines, proinflammatory mediators, and proinflammatory enzymes. In the CNS, cytokines such as IL-3 and IL-6 initiate microglial activation and are also produced by activated microglia. In combination with a resultant recruitment of blood-derived immune cells, the CNS inflammatory response is heightened and promotes neuronal damage (Shabab, Khanabdali, Moghadamtousi, Kadir, & Mohan, 2017; Soto & Howell, 2014). Disruption of the BBB facilitates these processes, as microglia can be exposed to several pro-inflammatory agents and activating molecules via recognition by toll-like receptors (TLRs) on the microglial surface (Bazan et al., 2012).

ONH RGCs and glial cells have a rapid and early response to glaucomatous insults, such as increased IOP. Astrocyte reactivity has been noted in the ONH and retina in human glaucoma and within the early stages of experimental glaucoma (Hernandez, Miao, & Lukas, 2008; Soto & Howell, 2014). A short term IOP increase causes rapid and reversible morphological astrocyte changes within the ONH, such as hypertrophy and process retraction (Sun, Qu, & Jakobs, 2013).

In the setting of glaucoma, astrocytes can overexpress cell adhesion proteins, thus promoting immune cell adhesion and migration to sites of damage in the ONH. In human glaucoma and animal models, ONH astrocytes upregulate tenascin-C (extracellular matrix glycoprotein that uses TLR4 signaling to reinforce proinflammatory responses). This phenomenon indicates astrocytes in glaucoma may have a proinflammatory role (Soto & Howell, 2014).

The inflammatory processes mediated by astrocytes, microglia, and infiltrating monocytes have a critical role in glaucoma progression. Microglial activation in the ONH

and retina has been noted in experimental glaucoma models (high IOP, DBA/2J). Increased proliferation, phagocytic activity, proinflammatory molecule expression, and morphological changes are indicative of microglial activation. The degree of microglia activation is linked to ONH axon degeneration, but the role of microglia in glaucoma advancement is not elucidated (Soto & Howell, 2014).

Upregulation of several genes associated with inflammatory pathways in the ONH and retina has been noted in an inherited model of glaucoma using DBA/2J mice. The molecular changes occurred prior to detectable RGC and axon loss. Genes linked with leukocyte activation, chemotaxis, and the immune response were upregulated earlier in high IOP models that lacked detectable axon loss. Note that neuroinflammatory processes can be beneficial or deleterious, thus confounding efforts to develop neuroprotective therapies that target these processes (Soto & Howell, 2014).

## Chapter II.

### Materials and Methods

#### *Animal husbandry*

All animal experiments were performed in accordance with the Statement for the Use of Animals in Ophthalmic and Vision Research of the Association for Research in Vision and Ophthalmology and were approved by the Institutional Animal Care and Use Committee of Schepens Eye Research Institute. Adult male and female C57BL/6 mice were obtained from the Jackson Laboratory (Bar Harbor, ME, stock# 000664). C57BL/6 pups (postnatal day 3-4) were used as well to extract astrocytes for cell culture. DBA/2J mice (Jackson Laboratory, stock# 000671) were aged to 15 months in our animal facility. Iris stromal atrophy, pigment dispersion, and the subsequent blockage of the aqueous humor drainage structures lead to the development of pigmentary glaucoma in this strain (Bouhenni et al., 2012; Libby et al., 2005). All mice were group housed on a 12 hour light/dark cycle and had access to water and food *ad libitum*. Age-matched male and female mice were used in equal ratios for the microbead experiments.

#### *Retro-orbital optic nerve crush (ONC)*

Mice were put under general anesthesia by intraperitoneal injection with ketamine and xylazine (100 mg/kg and 20 mg/kg body weight, respectively). Topical anesthetic (0.5% proparacaine) was applied to the cornea of the experimental (right) eye prior to the procedure. Artificial tears were applied to the left eye to keep the corneal surface moist.

The retrobulbar optic nerve was exposed using blunt dissection through a small incision made in the conjunctiva temporally. The nerve of the right eye was then crushed approximately 0.5 mm behind the globe for 10 seconds with self-closing forceps (Sun et al., 2010). Time points for tissue extraction were 4 hours, 24 hours, 1 week, and 3 weeks after the crush was performed.

*Microbead occlusion model of ocular hypertension (OHT)*

The IOP was elevated unilaterally by injection of microbeads into the anterior chamber of the right eye (Sappington et al., 2010). Polystyrene microbeads (FluoSpheres polystyrene, 15 µm diameter, orange, Invitrogen, Carlsbad, CA) were suspended in sterile saline solution at a final concentration of  $2.7 \times 10^7$  beads/mL. The final concentration of the magnetic bead solution in sterile saline solution was  $1.6 \times 10^9$  beads/mL. The respective microbead solutions was injected into the eye with a glass micropipette attached to a Hamilton syringe. The micropipettes were pulled from borosilicate glass capillaries (1.5/0.84 mm OD/ID without filament; World Precision Instruments, Sarasota, FL) using an electrode puller (Sutter Instruments Co., Novato, CA). The tips were trimmed with fine tweezers to a lumen size of approximately 30-50 µm.

Prior to beginning the procedure, the mice were put under general anesthesia via intraperitoneal injection with ketamine and xylazine (100 mg/kg and 20 mg/kg body weight, respectively). Topical anesthetic (0.5% proparacaine) was applied to the right eye prior to commencing the procedure. Artificial tears were applied to the contralateral, untreated (control) eye to prevent drying of the corneal surface. The eyelids were retracted with forceps, and a pilot hole was made in the cornea with a ½ inch 30G needle,

slightly off-center in relation to the pupil. An air bubble was created using a micropipette attached to a Hamilton syringe via polyethylene tubing backfilled with mineral oil. Precautions were taken to prevent striking the lens surface with the 30G needle or micropipette while entering the AC. 2-3  $\mu$ L of microbead solution was injected into the AC of each eye. Control mice were injected with an equivalent volume of sterile saline in their left eye.

#### *Measurement of intraocular pressure (IOP)*

The IOP was non-invasively measured at baseline and twice weekly after injection of microbeads with a rebound tonometer (TonoLab, Espoo, Finland). Measurements were also taken in the non-treated contralateral (control) eye. The tonometer itself provides an IOP reading by rapidly measuring the pressure six consecutive times. The recorded IOPs were the average of five mean values obtained from the tonometer. IOPs were taken on mice lightly anesthetized with isoflurane. The anesthesia was induced in a chamber with 3% isoflurane and oxygen. The mouse was then switched to a nose cone supplied with 1.5% isoflurane and oxygen. The mouse was then placed on a small platform, and the IOP was measured. Time points for IOP measurement were immediately prior to microbead injection (baseline) and every 3 or 4 days subsequent to injection. Measurements were taken within the same time frame of the day to minimize circadian variation. Five measurements were taken per eye and averaged to obtain a mean value. The cumulative IOP (cIOP), defined as the difference between the area under the IOP curve over time for the experimental and control eyes, was calculated using a user-written Matlab (Mathworks, Natick, MA) program.

### *Tissue collection and processing*

Mouse heads were fixed in 4% paraformaldehyde in PBS for 2 hours following CO<sub>2</sub> asphyxiation and cervical dislocation. The heads were then washed 2 to 3 times in PBS. Following careful opening of the skull and removal of the brain, the eye globe with its attached optic nerve was excised from the orbital bones and remaining ocular tissues. The dura surrounding the optic nerve was removed. The cornea was removed by cutting along the limbus, followed by the lens and vitreous. The sclera and retinal pigment epithelium were gently separated from the retina. The optic nerve and nerve head were dissected from the globes, leaving a small section of retina attached. Both the optic nerve and nerve head were immersed in 30% sucrose in PBS solution overnight at 4 °C. The optic nerves and nerve heads were embedded in tissue-freezing medium (TFM, General Data Healthcare, Cincinnati, OH). The tissue was sectioned at 14-16 µm thicknesses in a transverse or longitudinal orientation using a Leica CM3050 S cryostat.

### *Immunohistochemistry (IHC)*

Sections were blocked with 4% normal donkey serum (Jackson ImmunoResearch) and 0.1% TritonX100 in PBS for 30 minutes, incubated with primary antibodies overnight and secondary antibodies for 2 hours in the same blocking solution, and mounted with Vectashield mounting medium. The primary antibodies used in this study were: chicken anti-GFAP (1:400, Abcam), rabbit anti-SMI32 (1:50, Millipore), rabbit anti-IBA1 (1:200, Wako), goat anti-mLipocalin-2/NGAL (1:200, R&D Systems), rabbit anti-Tau (1:100, Abcam), and rabbit anti-CD3 (1:200, Abcam). All fluorescent secondary antibodies were purchased from Jackson ImmunoResearch and were used at 1:400.

### *Image acquisition and analysis*

Images were taken on a Leica SP5 laser scanning confocal microscope (Leica Biosystems).

### *In situ hybridization (ISH)*

Optic nerves were dissected 4 hours or 1 day after optic nerve crush, embedded in TFM, cryosectioned at 14-16  $\mu\text{m}$  longitudinally, and fixed with cold 4% PFA on the slides for 15 minutes. *In situ* hybridization was carried out using RNAscope® 2.5 HD Detection Reagent - RED (322360-USM, Advanced Cell Diagnostics) probes specific for Lcn2. Sections from uninjured optic nerves were included as controls.

### *Astrocyte Collection, RNA extraction, and cDNA synthesis*

RNA samples were extracted from cultured astrocytes collected from the ONH of day 3 to day 4 C57BL/6 pups. The tissue was digested by incubating with 0.25% trypsin and 0.01% DNase in cell culture medium (Dulbecco's Modified Eagle Medium, DMEM), followed by mechanical trituration. Cells were plated on polylysine-coated coverslips in DMEM/F-12 supplemented with 10% fetal bovine serum (FBS) at  $1.5\text{-}3 \times 10^7$  cells/cm<sup>2</sup>. After 7-10 days in culture, the plates were shaken at 200 rpm for 18h to remove most oligodendrocytes and microglia. The remaining cells were trypsinized and passaged. After 2 rounds of trypsinization and replating, >95% of the remaining cells are positive for the astrocyte marker GFAP (S. Li et al., 2017). The cells were then seeded in 6-well plates and incubated in 500 ng/mL murine Lcn2 (R&D Systems, Minneapolis, MN) for 24 h. Control cells were incubated in medium only. All measurements were

performed in triplicate. Cells were dissolved using 350  $\mu$ L of lysis buffer from the RNeasy Plus Micro Kit (Qiagen, 74034) and gently scraped from the cell-culture dish. Further extraction steps were followed per the manufacturer's protocol.

8  $\mu$ L of RNA was used for reverse transcription into cDNA by combining RNA samples with 1  $\mu$ L of a random hexamer mix and 1  $\mu$ L of dNTP mix, then incubated for 5 min at 65°C using an Applied Biosystems GeneAmp PCR System. 10  $\mu$ L of cDNA Synthesis Mix (Life Technologies, 18080-051) was added to each RNA/primer mix under the following conditions: 10 min at 25°C, 50 min at 50°C, and 5 min at 85°C. 1  $\mu$ L of RNase H was added to each sample, then incubated for 20 min at 37°C. The cDNA products were immediately used for qPCR.

#### *Quantitative PCR (qPCR)*

qPCR was performed using an Applied Biosystems StepOnePlus™ Real-Time PCR System and SYBR Green PCR Master Mix (Applied Biosystems) in 10  $\mu$ l reaction volumes with 5  $\mu$ M primer concentrations. GAPDH was used as a housekeeping gene. Several primers for markers of inflammation and astrocyte reactivity (Table 1) were used under the following PCR conditions: 10 min at 95°C, 40 cycles of 15 sec at 95°C, then 1 min at 60°C, 15 sec at 95°C, then 1 min at 60°C. The primer sequences were obtained from PrimerBank (Spandidos, Wang, Wang, & Seed, 2010) or designed using a web-based tool, Primer3 (Cherry et al., 2012).

### *Statistical Analysis*

Quantitative values for the microbead experiments are shown as the mean of the data set  $\pm$  standard deviation (SD). P-values were significant if  $\leq 0.05$ . qPCR quantitative values were reported as the mean  $\pm$  standard error of the mean (SEM). Correction was performed using the Bonferroni method given the number of comparisons done. P-values  $\leq 0.0025$  were significant. A two-tailed t-test was used to analyze all data sets.

## Chapter III

### Results

#### Lcn2 in the Crushed Optic Nerve

##### Immunohistochemistry

Reactive gliosis induced by ONC triggers upregulation of Lcn2 and several other genes immediately after crush, with attenuated expression over time as evidenced by DNA microarray analysis (Qu & Jakobs, 2013). A correlation between ONC and Lcn2 expression in the crushed optic nerve was investigated via immunohistochemistry of optic nerve sections. Time points were 4 h, 1 d, and 7 d following ONC.

4 h following ONC, Lcn2<sup>+</sup> cells that are small and round in appearance are first localized to the vessels of the pia mater (the sheath where blood vessels that nourish the ON are located) [Figure 1]. Some cells are also noted in what are most likely blood vessels more central to the nerve. 1 d after crush, Lcn2<sup>+</sup> cells leave the blood vessels to invade the crush site, a behavior exhibited by T-cells. By day 7 after crush, a cell population is localized to the lesion area, and Lcn2 staining appears reduced. IHC was also conducted using antibodies for microglia/macrophages (Iba1) and astrocytes (GFAP). These cells were not positive for either, thus indicating that the cells are not astrocytes or microglia. Due to presentation of cells within the vasculature, a counterstain with CD3 was done, revealing co-localization with Lcn2. This suggests that the Lcn2<sup>+</sup> cells may be T-cells.

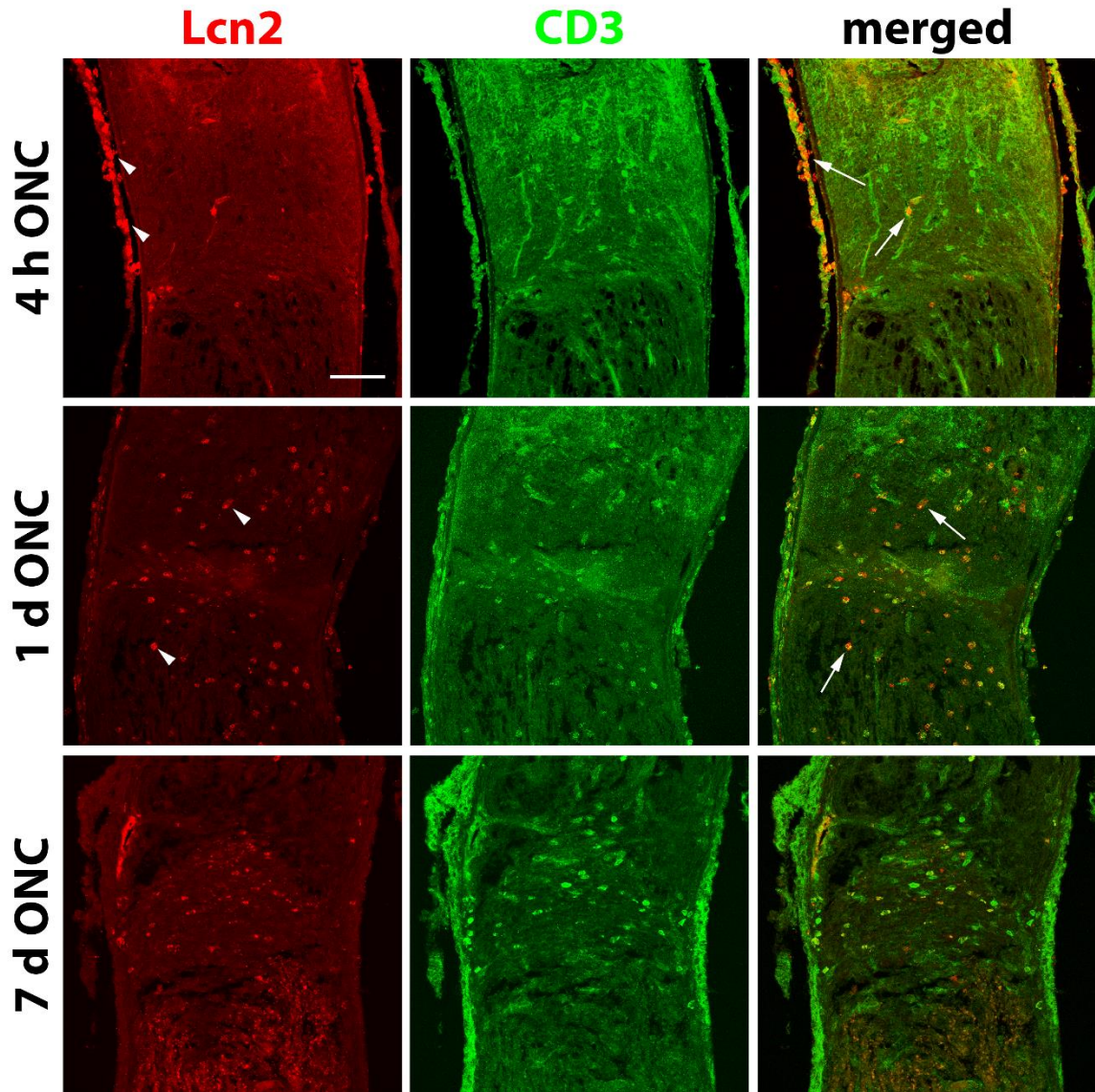


Figure 4. Longitudinal optic nerve tissue sections labeled for Lcn2 and the T-cell marker, CD3, following optic nerve crush.

*Images were taken 4 h, 1 d, and 7 d after crush. Co-localization of CD3 and Lcn2 was noted. Arrowheads point out Lcn2+ cells. Co-labeled cells are shown in the last column of the figure (arrows). Scale bar = 50  $\mu$ m.*

### *In situ* hybridization

*In situ* hybridization was used to validate the IHC findings, as the Lcn2 antibody may not necessarily reveal the site of Lcn2 production. Expression of Lcn2 was localized to the pia mater and the blood vessels proximally located to the ONH starting at 4h following ONC. More robust and generalized expression was observed 1 d following crush. After 1 d, Lcn2 expression was observed at the distal most part of the ON (Figure 5). The ISH findings support those observed in the IHC experiment.

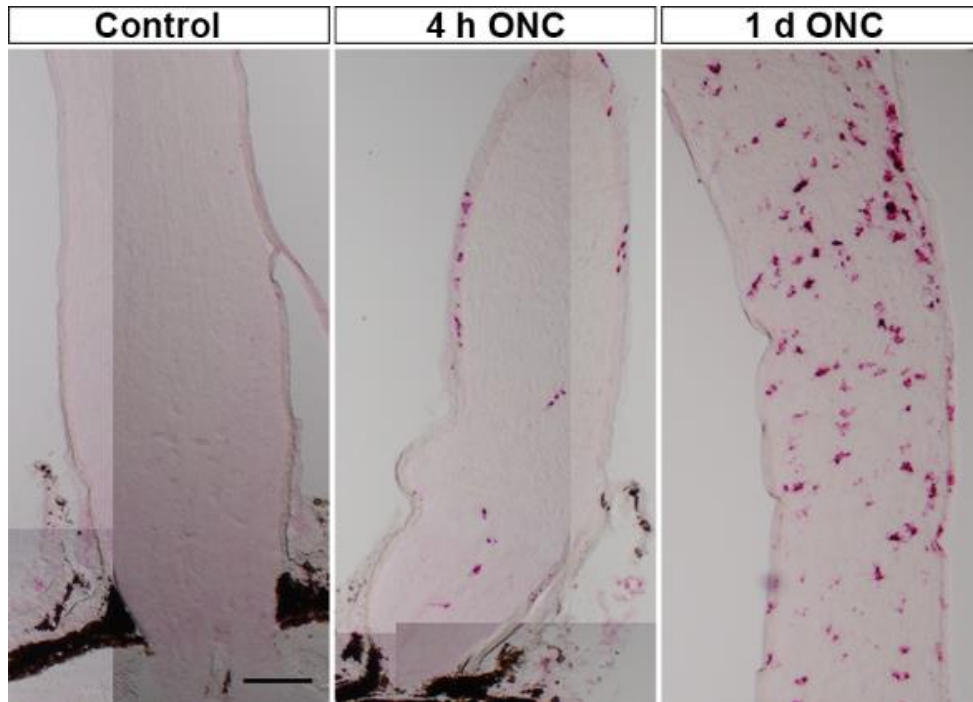


Figure 5. *In situ* hybridization staining of Lcn2 in the optic nerve.

*Longitudinal section. 4 h after ONC, Lcn2 expression (red dots) is detected in the blood vessels and pia mater (arrowheads). Ubiquitous expression occurs by 1 d after ONC. Scale bar = 100  $\mu$ m.*

## Microbead Occlusion Model of Ocular Hypertension

27 C57BL/6 mice were injected with microbeads (polystyrene or magnetic) in the right eye to induce IOP elevation. Young adult mice (aged 2 to 4 months) were used at the beginning of the experiment. The contralateral eye was injected with sterile saline solution as a control. This was done to rule out any possible effect of the injection itself. The IOP was measured every 3 to 4 days following injection over a period of 1 month. Overall, the IOP trend following injection revealed that IOP remained at baseline in the control (saline-injected) eyes, while IOP increased over the course of the experiment in microbead-injected eyes (Figure 6a).

The cumulative IOP (cIOP) (measured in mmHg days) was used to account for the time course of IOP fluctuation between individual animals. cIOP is defined as the difference between the area under the IOP curve over time for the experimental and control eyes. The cIOP was  $80.0 \pm 8.86$  mm Hg days (mean  $\pm$  SD) for the microbead-injected eyes, which was higher than for the saline-injected eyes in the 1 week group ( $64.7 \pm 2.23$ ,  $p < 0.01$ ,  $n = 6$ , Figure 6c). The same trend was noted in the 1 month group (microbead-injected eyes,  $362.4 \pm 59.28$  & saline-injected eyes ( $266.2 \pm 8.43$ ,  $p < 0.001$ ,  $n = 8$ , Figure 6e). Maximal IOP elevation was noted approximately 7 days following microbead injection (Figure 6a). These results held true for the experiment conducted with magnetic beads as well (Figure 6b,d,f). Experiments were performed using magnetic beads to determine if the process of microbead injection would be facilitated or yield more consistent results. However, the use of magnetic beads did not prove advantageous (Figure 6b,d,f).

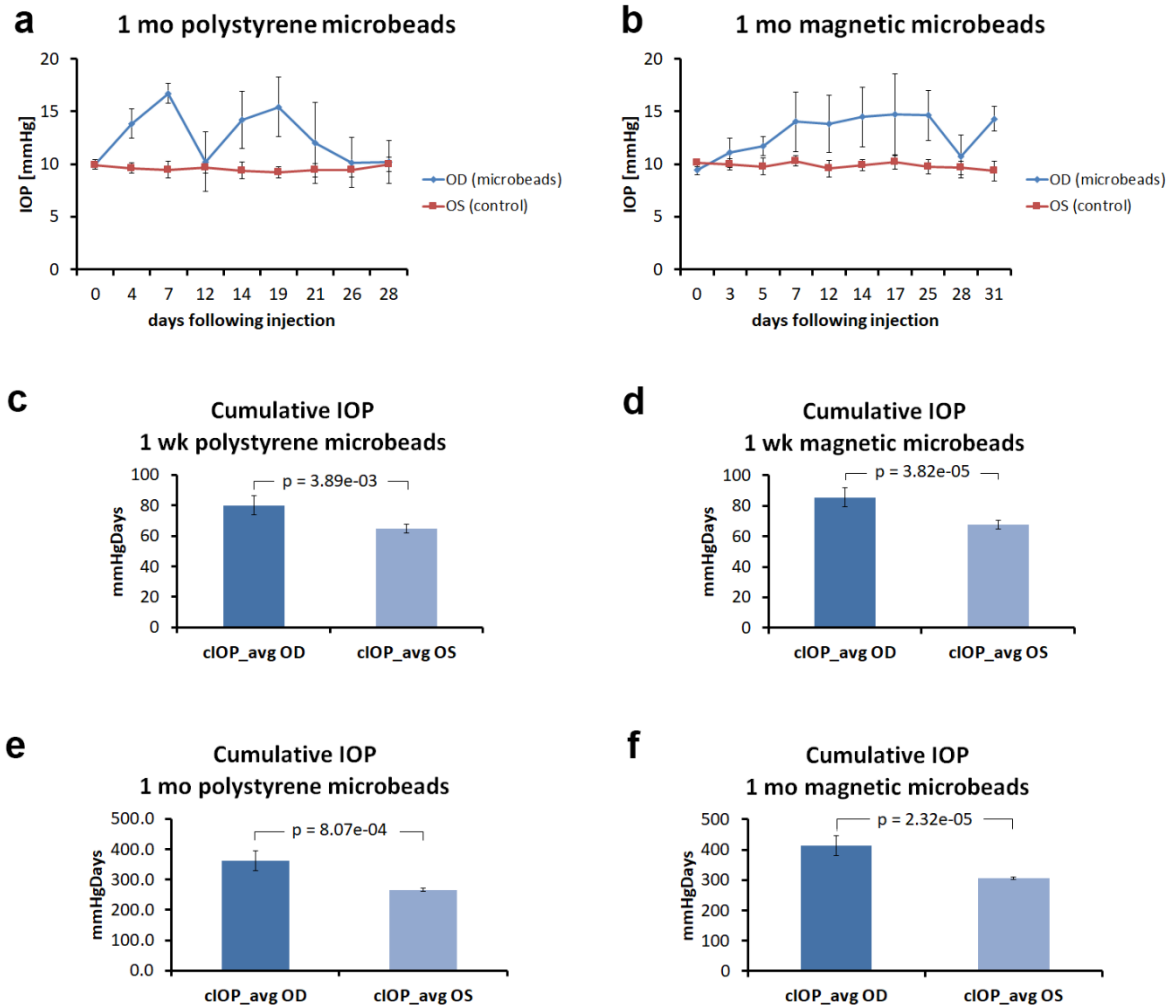


Figure 6. Ocular hypertension induced via microbead injection.

**a-b**, An IOP peak was noted at approximately 7 days following microbead injection. The IOP remained at baseline in the contralateral eye throughout the course of the experiment. **c-f**, The area under the IOP curve (**c-f**). The overall trend was that there was a statistically significant IOP elevation in the treated (right) eye.  $p < 0.05$ ; two-tailed  $t$ -test. **a,e**,  $n = 8$ ; **b,c,f**,  $n = 6$ ; **d**,  $n = 7$ . Data presented as the mean  $\pm$  SD.

To determine if there is an association between elevated IOP and Lcn2 ON expression, immunohistochemistry of ON sections was done. For microbead injection, the chosen time points were 1 week and 4 weeks following the procedure. Sections were counterstained with DAPI and CD3. However, no Lcn2+ or CD3+ cells were noted (Figure 7). There was also no Lcn2 or CD3 staining noted on the 4 week nerve sections (image not shown).

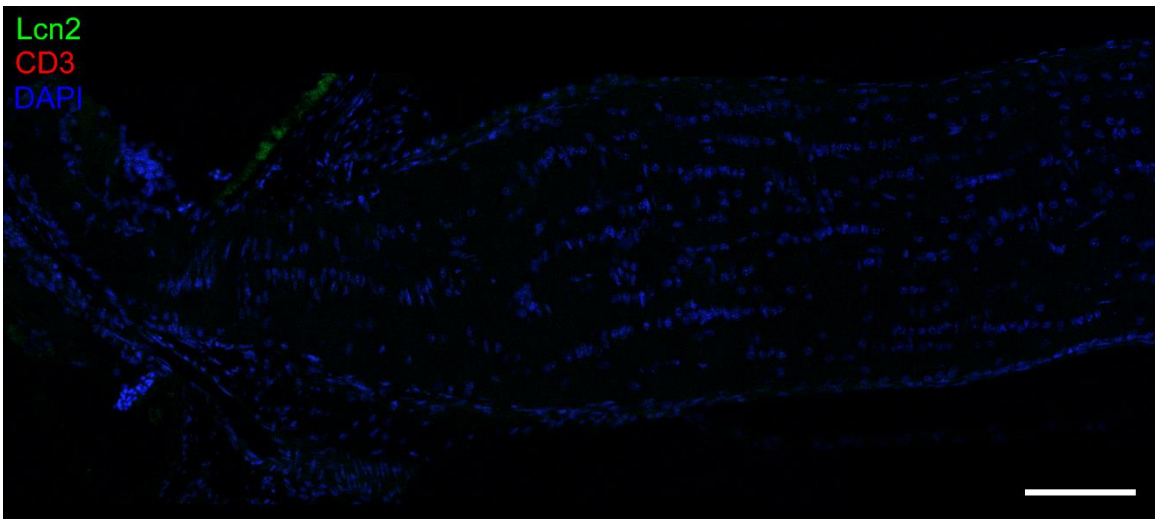


Figure 7. Immunohistochemistry in the ON following microbead injection.

*Longitudinal optic nerve section 1 w following magnetic microbead injection (1 of n = 7). DAPI stain with background Lcn2 staining noted. Scale bar, 100  $\mu$ m.*

#### Lcn2 in DBA/2J

IHC was also performed using ON sections obtained from DBA/2J mice aged between 4 and 15 m at time of death. At 4 m (pre glaucoma), counterstaining with Lcn2 and CD3 did not reveal any labeled cells (Figure 8a). By 9 m (mild glaucoma) and 15 m

(severe glaucoma), Lcn2+ cells were observed in the pia and within the optic nerve (Figure 8b-c). Lcn2 was not found to co-localize with GFAP, SMI-32 (RGC label), Iba1, or Tau (RGC axon label) at any stage of glaucoma in the DBA model (imaging not shown).

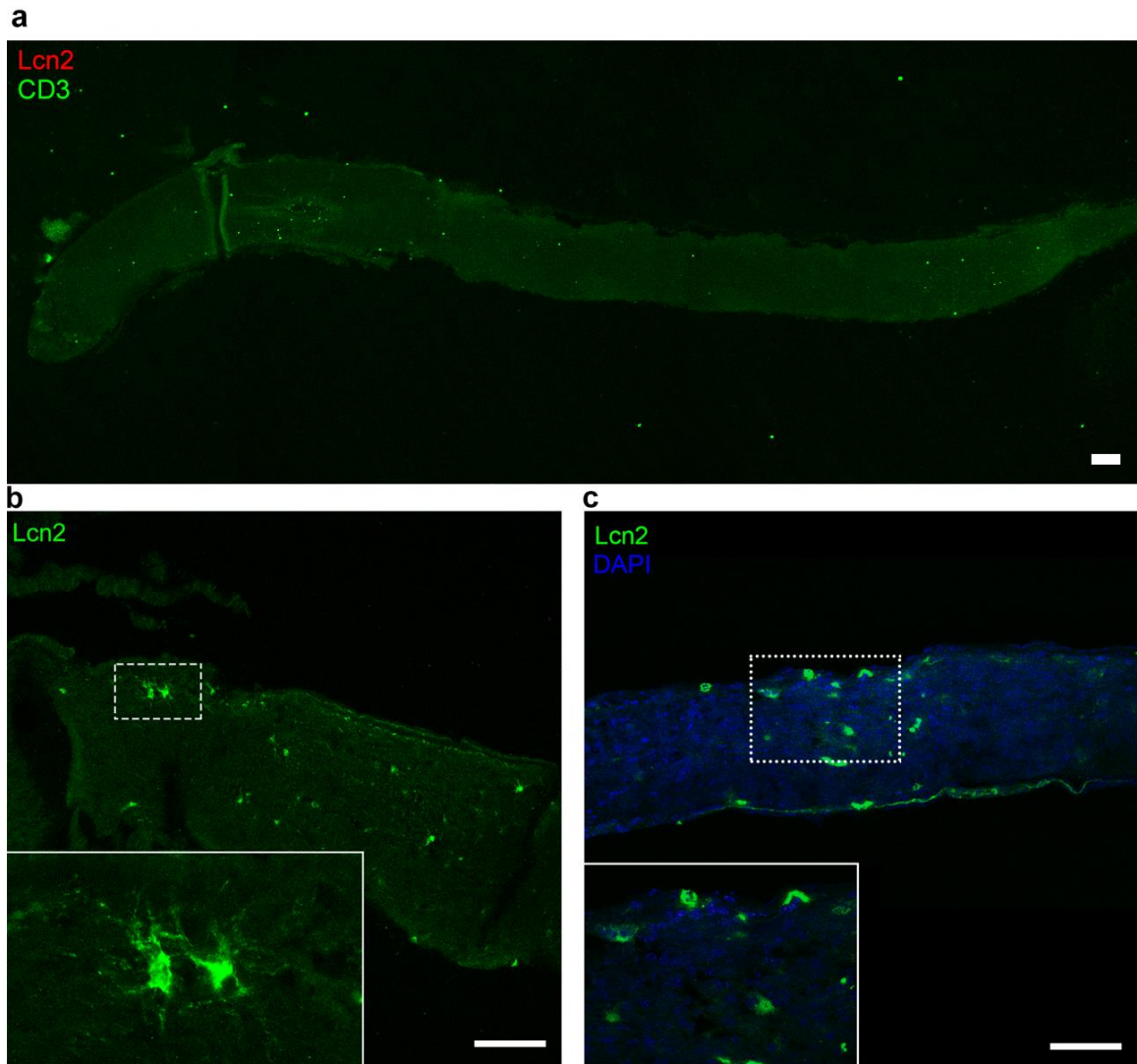


Figure 8. Immunohistochemistry of optic nerves from DBA/2J mice.

*Longitudinal section. No Lcn2 or CD3 staining was noted at 4 m of age (a). Lcn2+ staining was noted in 9 m old (b), and 15 m old (c) mice. The insets (b-c) are enlargements of the dashed squares. Scale bar, 100  $\mu$ m.*

### qPCR Analysis of Lcn2 Regulation in Cultured Astrocytes

A qPCR screen of cultured astrocytes collected from the ONH of day 3 to day 4 C57BL/6 pups was performed to determine the impact of Lcn2 on reactive astrocyte gene expression. Non-treated cells were used as controls. Findings from Liddelow et al. (2017) show that neuroinflammation and ischemia induce A1 (neurotoxic) and A2 (neuroprotective) reactive astrocytes. This was the basis for using A1 and A2 markers in the screen. However, it was found that the majority of A1 & A2 astrocyte markers are not differentially regulated when cultured with Lcn2 (Figure 9a-b). The inflammatory marker,  $TNF\alpha$ , was differentially upregulated by Lcn2 as expected (Figure 9c). Statistical significance ( $p < 0.0025$ ) was calculated using a two-tailed t-test that accounted for multiple comparisons with the Bonferroni correction.

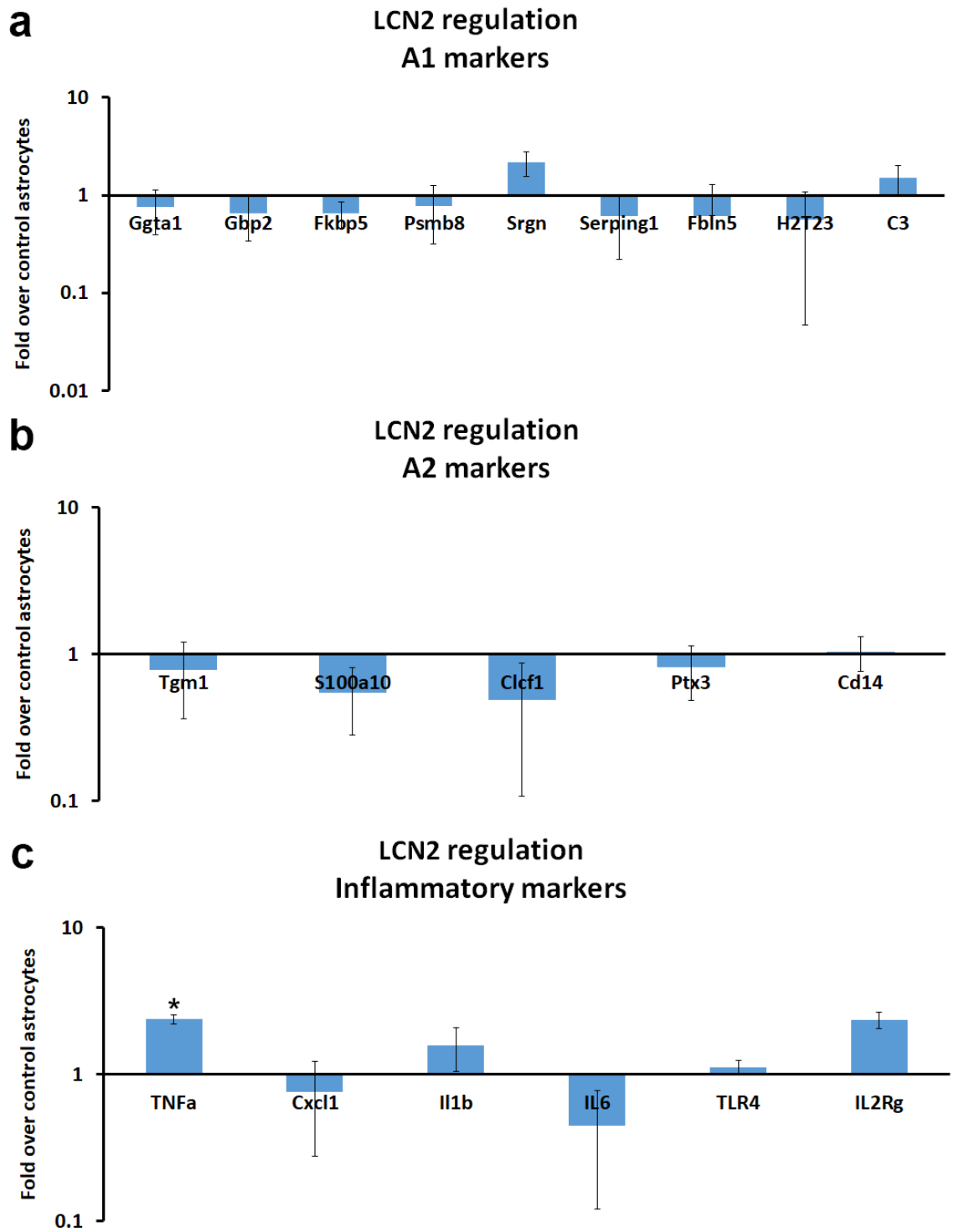


Figure 9. qPCR for markers of astrocyte reactivity and neuroinflammation.

$n = 3$ . *TNFa* was differentially regulated (c). \* =  $p < 0.0025$ ; two-tailed *t*-test with Bonferroni correction. Data presented as the mean  $\pm$  SEM.

## Chapter IV

### Discussion

Remodeling of ON astrocytes has been noted in models of glaucoma as well as optic nerve and CNS injuries (Liddelow et al., 2017; Sun et al., 2010). It was previously thought that astrocyte reactivity was solely neurotoxic, but recent findings demonstrate that reactive astrocytes can prove neuroprotective as well (Liddelow et al., 2017; Sofroniew, 2014; Sun et al., 2017). Astrocyte reactivity is typically diagnosed based on morphological changes (process thickening and reorientation), but can also be tracked genomically (Qu & Jakobs, 2013; Zamanian et al., 2012). *Lcn2* upregulation has been reported in the aforementioned disease and injury models, suggesting that it may be a general marker for astrocyte reactivity. This led us to investigate its potential link to astrocyte reactivity in a glaucoma context.

We found that *Lcn2* mRNA is upregulated in the optic nerves of the ONC and DBA/2J models, but not following microbead injection. Gene upregulation can be induced by a resident cell population, or an influx of cells that are not native to the ONH environment. As such, localization experiments (IHC and ISH) were performed. The localization of *Lcn2*<sup>+</sup> cells within the pia mater and blood vessels of the optic nerve was noted with IHC and validated via ISH. IHC revealed *Lcn2*<sup>+</sup> cells following ONC that co-label with CD3. In ONH-derived astrocytes, TNF- $\alpha$  was upregulated by *Lcn2*.

Optic nerve crush was used to induce robust astrocyte reactivity, a process that precipitates differential regulation of ONH genes involved in inflammation and immunity (Qu & Jakobs, 2013). This rudimentary model of glaucomatous injury also has an inflammatory component that is secondary to the physical insult imparted upon the ON

(Rovere et al., 2016). Our IHC results showed Lcn2<sup>+</sup> cells that appeared to migrate towards the crush site by 1 d following ONC. By the seventh day, there was a decreased number of Lcn2<sup>+</sup> cells noted, which may be ascribed to cell migration to a different region of the optic nerve. In combination with the finding that the Lcn2<sup>+</sup> cell population was also CD3<sup>+</sup>, did not co-localize with GFAP or Iba1, and was migratory, it is likely that the cells were T-cells rather than reactive astrocytes or microglia. The round, small appearance of the cells also differs from the morphology of reactive astrocytes that possess ramified and hypertrophied processes (Sun et al., 2010).

The DBA/2J glaucoma model utilized also upregulates inflammatory genes, a common thread shared with the ONC model (Qu & Jakobs, 2013). The DBA mice share features found in human glaucoma: (a) age-dependency, (b) slow disease progression, and (c) asymmetric onset between the eyes (Bouhenni et al., 2012). However, the observed pigmentary changes in the anterior chamber are not a component of the most common form of glaucoma (POAG). Though the mouse model is grossly analogous to the human counterpart of pigmentary glaucoma, the latter lacks mutations for TYRP1 and GPNMB (Yang et al., 2018).

The microbead/ocular hypertension model aims to reproduce the high IOP element of glaucoma. Approximately 22-25% RGC axon loss has been reported 3 to 6 weeks following injection (Ito, Belforte, Cueva Vargas, & Di Polo, 2016). However, this loss does not appear to be attributed to Lcn2 upregulation as demonstrated by IHC for Lcn2 conducted 1 and 4 weeks after injection. A gene expression screen conducted with RNA-sequencing of ONs collected from microbead-treated mice confirms that Lcn2 is not differentially upregulated in this model (Zhu, manuscript submitted). The apparent

absence of inflammation in response to the high IOP insult in the microbead model suggests that the DBA and ONC models impart glaucomatous losses via differing mechanisms that are not well elucidated. Anderson, Libby, Gould, Smith, and John (2005) and Howell et al. (2012) showed that irradiation treatment of the optic nerve head offered protection to the optic nerve and retina from glaucomatous damage in DBA. Irradiation treatment was not neuroprotective to optic nerves exposed to chronically elevated IOP induced by an episcleral vein saline injection (Johnson, Cepurna, Choi, Choe, & Morrison, 2014). Based on their findings, glaucomatous damage likely involves the influx of monocytes into the optic nerve (Howell et al., 2012).

In finding that Lcn2<sup>+</sup> cells were not reactive astrocytes, we rejected our hypothesis of Lcn2 being an astrocyte reactivity marker in the optic nerve. We cultured purified ONH astrocytes and incubated them in Lcn2 to determine if astrocytes could be impelled to adopt a neurotoxic or neuroprotective phenotype. These were classified as A1 and A2 reactive astrocytes, respectively (Liddelow et al., 2017). We discovered that the A1 and A2 markers were not differentially regulated by Lcn2, but did upregulate TNF- $\alpha$  in astrocytes.

TNF- $\alpha$  is a proinflammatory cytokine that has been implicated in the propagation of glaucomatous neurodegeneration associated with IOP elevation. Reactive microglia have been linked to the mechanism employed by TNF- $\alpha$  to mediate RGC cytotoxicity induced by OHT induced via laser irradiation-induced angle closure (Nakazawa et al., 2006) or episcleral vein cauterization (Roh et al., 2012). The use of a TNF- $\alpha$  antagonist, Etanercept was used by Roh et al. (2012) to study the potential impact on OHT-associated RGC loss and inflammation. Reported results included cessation of RGC axon

degeneration, prevention of amoeboid-shaped microglia infiltration to the ONH, and reduced TNF- $\alpha$  and CD3 co-labeling secondary to diminished TNF- $\alpha$  levels in Etanercept-treated OHT rats (Roh et al., 2012).

The protective effect of Etanercept in the laser-induced angle closure models suggests that Iba1+ microglia can damage ganglion cells by secreting TNF- $\alpha$ . Microglial activation is also observed following ONC and in DBA mice (data not shown). Given the absence of Iba1+ and Lcn2 IHC co-labeling, we did not specifically address microglia in our study. However, optic nerve astrocytes can also produce TNF- $\alpha$  when stimulated with Lcn2. Examining the role of TNF- $\alpha$  and Lcn2 expression in the retina and astrocytes isolated from LCN2 knockout-DBA/2J or qPCR analysis of ONC tissues may prove insightful.

Due to the complexity of the disease, creation of an accurate glaucoma model that comprehensively mimics the human disease is difficult. One confounding factor in the microbead model was the degree of IOP elevation induced during the study. Sappington et al. (2010) have reported the IOP-lowering effect of anesthetics. This phenomenon is unavoidable, as measuring IOP in non-anesthetized mice is difficult. Another limitation of the high IOP model was the measurement device itself (TonoLab rebound tonometer). Compared to Goldmann applanation tonometry, rebound tonometry records lower IOP values in glaucoma patients (Tamcelik, Atalay, Cicik, & Ozkok, 2015).

During the 1 mo polystyrene microbead experiment, a dip in the average IOP was noted at day 12 following injection. The IOP increased again by days 14 & 19, and tapered off back to baseline at subsequent time points (Figure 6a). This unexpected finding is likely due to measuring or instrumentation error. IOPs were also measured

within the same time frame to mitigate the effect of circadian rhythm. This limited snapshot precludes the recording of any IOP spikes outside the recording window.

Reactivity and subsequent dedifferentiation are initiated with repeated serial passaging of cultured astrocytes. As such, the cells were used after the second or third passage. However, cultured astrocytes also respond differently compared to in vivo astrocytes due to the absence of a 3D growth environment (Pekny & Pekna, 2014). Future experiments could investigate the effect of intravitreally or intracamerally injected Lcn2 on ONH astrocytes or study cultured astrocytes in a 3D culture environment. The results from our qPCR A1/A2 astrocyte marker screen (Figure 9a-b) indicate that though both are part of the CNS, the brain and ON respond to insults in different manner, thus offering another avenue for further investigation. The suggested association between Lcn2 and TNF- $\alpha$  and their potential as therapeutic targets that aim to attenuate ON inflammatory damage may facilitate the development of additional topical therapies.

Appendix 1.

qPCR Primer Sequences

	Gene Name	Forward	Reverse
Internal control	Gapdh	5'- GGTTGTCTCCTGCGA CTTCAA-3'	5'- CCTGTTGCTGTAGCCG TATTCAT-3'
Astrocyte marker	Gfap	5'- CACGAACGAGTCCCT AGAGC-3'	5'- ATGGTGATGCGGTTTT CTTC-3'
A1	C3	5'- CCAGCTCCCCATTAG CTCTG-3'	5'- GCACTTGCCTCTTTAG GAAGTC-3'
A1	Fbln5	5'- GCTTGTCGTGGGGAC ATGAT-3'	5'- TGGGGTAGTTGGAAGC TGGTA-3'
A1	Fkbp5	5'- TGAGGGCACCAGTAA CAATGG-3'	5'- CAACATCCCTTTGTAG TGGACAT-3'
A1	Gbp2	5'- CTGCACTATGTGACG GAGCTA-3'	5'- GAGTCCACACAAAGG TTGAAA-3'
A1	Ggta1	5'- GGTGGTTCCCAAGCT GGTTTA-3'	5'- CGGGCGGTTCTTTGGA TTGA-3'

	Gene Name	Forward	Reverse
A1	H2-T23	5'- ACAGTCCCGACCCAG AGTAG-3'	5'- CCACGTAGCCGACAAT GATGA-3'
A1	Psmb8	5'- ATGGCGTTACTGGAT CTGTGC-3'	5'- CGCGGAGAACTGTA GTGTCC-3'
A1	Serping1	5'- TAGAGCCTTCTCAGA TCCCGA-3'	5'- ACTCGTTGGCTACTTT ACCCA-3'
A1	Srgn	5'- CTCGCCTTCGTCCTGG TTT-3'	5'- CCTCGATGCAGTTCGC AAAAA-3'
A2	Cd14	5'- CTCTGTCCTTAAAGC GGCTTAC-3'	5'- GTTGCGGAGGTTCAAG ATGTT-3'
A2	Clefl	5'- GACTCGTGGGGGATG TTAGC-3'	5'- CTAAGCTGCGGAGTTG ATGCT-3'
A2	Emp1	5'- TTGGTGCTACTGGCT GGTCT-3'	5'- CATTGCCGTAGGACAG GGAG-3'
A2	Ptx3	5'- CCTGCGATCCTGCTTT GTG-3'	5'- GGTGGGATGAAGTCC ATTGTC-3'
A2	S100a10	5'- TGGAACCATGATGC TTACGTT-3'	5'- GAAGCCCACTTTGCCA TCTC-3'

	Gene Name	Forward	Reverse
A2	Tgm1	5'- TCTGGGCTCGTTGTTG TGG-3'	5'- AACCAGCATTCCCTCT CGGA-3'
Inflammation	Cxcl1	5'- CTGGGATTCACCTCA AGAACATC-3'	5'- CAGGGTCAAGGCAAG CCTC-3'
Inflammation	Il1b	5'- GAAATGCCACCTTTT GACAGTG-3'	5'- TGGATGCTCTCATCAG GACAG-3'
Inflammation	Il6	5'- TAGTCCTTCCTACCCC AATTTCC-3'	5'- TTGGTCCTTAGCCACT CCTTC-3'
Inflammation	Il2rg	5'- CTCAGGCAACCAACC TCAC-3'	5'- GCTGGACAACAAATGT CTGGTAG-3'
Inflammation	Tlr4	5'- ATGGCATGGCTTACA CCACC-3'	5'- GAGGCCAATTTGTCT CCACA-3'
Inflammation	Tnf- $\alpha$	5'- CCTGTAGCCCACGTC GTAG-3'	5'- GGGAGTAGACAAGGT ACAACCC-3'

Table 1. List of qPCR Primer Sequences used to screen for Lcn2 regulation in astrocytes isolated from C57BL/6 pups.

*Genes were chosen based on the previously reported activation of A1/A2 reactive astrocytes induced by CNS disease and injury (Liddelw, 2017).*

## References

- Abella, V., Scotece, M., Conde, J., Gomez, R., Lois, A., Pino, J., . . . Gualillo, O. (2015). The potential of lipocalin-2/NGAL as biomarker for inflammatory and metabolic diseases. *Biomarkers*, *20*(8), 565-571. doi:10.3109/1354750X.2015.1123354
- Anderson, M. G., Libby, R. T., Gould, D. B., Smith, R. S., & John, S. W. (2005). High-dose radiation with bone marrow transfer prevents neurodegeneration in an inherited glaucoma. *Proc Natl Acad Sci U S A*, *102*(12), 4566-4571. doi:10.1073/pnas.0407357102
- Anderson, M. G., Smith, R. S., Hawes, N. L., Zabaleta, A., Chang, B., Wiggs, J. L., & John, S. W. (2002). Mutations in genes encoding melanosomal proteins cause pigmentary glaucoma in DBA/2J mice. *Nat Genet*, *30*(1), 81-85. doi:10.1038/ng794
- Bazan, N. G., Halabi, A., Ertel, M., & Petasis, N. A. (2012). Chapter 34 - Neuroinflammation. In S. T. Brady, G. J. Siegel, R. W. Albers, & D. L. Price (Eds.), *Basic Neurochemistry (Eighth Edition)* (pp. 610-620). New York: Academic Press.
- Berard, J. L., Zarruk, J. G., Arbour, N., Prat, A., Yong, V. W., Jacques, F. H., . . . David, S. (2012). Lipocalin 2 is a novel immune mediator of experimental autoimmune encephalomyelitis pathogenesis and is modulated in multiple sclerosis. *Glia*, *60*(7), 1145-1159. doi:10.1002/glia.22342
- Bi, F., Huang, C., Tong, J., Qiu, G., Huang, B., Wu, Q., . . . Zhou, H. (2013). Reactive astrocytes secrete lcn2 to promote neuron death. *Proc Natl Acad Sci U S A*, *110*(10), 4069-4074. doi:10.1073/pnas.1218497110
- Bouhenni, R. A., Dunmire, J., Sewell, A., & Edward, D. P. (2012). Animal models of glaucoma. *J Biomed Biotechnol*, *2012*, 692609. doi:10.1155/2012/692609
- Braunger, B. M., Fuchshofer, R., & Tamm, E. R. (2015). The aqueous humor outflow pathways in glaucoma: A unifying concept of disease mechanisms and causative treatment. *Eur J Pharm Biopharm*, *95*(Pt B), 173-181. doi:10.1016/j.ejpb.2015.04.029
- Cherry, J. M., Hong, E. L., Amundsen, C., Balakrishnan, R., Binkley, G., Chan, E. T., . . . Wong, E. D. (2012). Saccharomyces Genome Database: the genomics resource of budding yeast. *Nucleic Acids Res*, *40*(Database issue), D700-705. doi:10.1093/nar/gkr1029

- Chun, B. Y., Kim, J. H., Nam, Y., Huh, M. I., Han, S., & Suk, K. (2015). Pathological Involvement of Astrocyte-Derived Lipocalin-2 in the Demyelinating Optic Neuritis. *Invest Ophthalmol Vis Sci*, *56*(6), 3691-3698. doi:10.1167/iovs.15-16851
- Crish, S. D., Sappington, R. M., Inman, D. M., Horner, P. J., & Calkins, D. J. (2010). Distal axonopathy with structural persistence in glaucomatous neurodegeneration. *Proc Natl Acad Sci U S A*, *107*(11), 5196-5201. doi:10.1073/pnas.0913141107
- Distelhorst, J. S., & Hughes, G. M. (2003). Open-angle glaucoma. *Am Fam Physician*, *67*(9), 1937-1944.
- Flammer, J., Orgul, S., Costa, V. P., Orzalesi, N., Krieglstein, G. K., Serra, L. M., . . . Stefansson, E. (2002). The impact of ocular blood flow in glaucoma. *Prog Retin Eye Res*, *21*(4), 359-393.
- Flo, T. H., Smith, K. D., Sato, S., Rodriguez, D. J., Holmes, M. A., Strong, R. K., . . . Aderem, A. (2004). Lipocalin 2 mediates an innate immune response to bacterial infection by sequestering iron. *Nature*, *432*(7019), 917-921. doi:10.1038/nature03104
- Hernandez, M. R., Miao, H., & Lukas, T. (2008). Astrocytes in glaucomatous optic neuropathy. *Prog Brain Res*, *173*, 353-373. doi:10.1016/S0079-6123(08)01125-4
- Howell, G. R., Macalinao, D. G., Sousa, G. L., Walden, M., Soto, I., Kneeland, S. C., . . . John, S. W. (2011). Molecular clustering identifies complement and endothelin induction as early events in a mouse model of glaucoma. *J Clin Invest*, *121*(4), 1429-1444. doi:10.1172/JCI44646
- Howell, G. R., Soto, I., Zhu, X., Ryan, M., Macalinao, D. G., Sousa, G. L., . . . John, S. W. (2012). Radiation treatment inhibits monocyte entry into the optic nerve head and prevents neuronal damage in a mouse model of glaucoma. *J Clin Invest*, *122*(4), 1246-1261. doi:10.1172/JCI61135
- Ito, Y. A., Belforte, N., Cueva Vargas, J. L., & Di Polo, A. (2016). A Magnetic Microbead Occlusion Model to Induce Ocular Hypertension-Dependent Glaucoma in Mice. *J Vis Exp*(109), e53731. doi:10.3791/53731
- Johnson, E. C., Cepurna, W. O., Choi, D., Choe, T. E., & Morrison, J. C. (2014). Radiation pretreatment does not protect the rat optic nerve from elevated intraocular pressure-induced injury. *Invest Ophthalmol Vis Sci*, *56*(1), 412-419. doi:10.1167/iovs.14-15094
- Kersey, T., Clement, C. I., Bloom, P., & Cordeiro, M. F. (2013). New trends in glaucoma risk, diagnosis & management. *Indian J Med Res*, *137*(4), 659-668.
- Kim, B. W., Jeong, K. H., Kim, J. H., Jin, M., Kim, J. H., Lee, M. G., . . . Suk, K. (2016). Pathogenic Upregulation of Glial Lipocalin-2 in the Parkinsonian Dopaminergic System. *J Neurosci*, *36*(20), 5608-5622. doi:10.1523/JNEUROSCI.4261-15.2016

- Kolb, H. (2011). Simple Anatomy of the Retina by Helga Kolb – Webvision. Retrieved from <https://webvision.med.utah.edu/book/part-i-foundations/simple-anatomy-of-the-retina/>
- Krishnan, A., Fei, F., Jones, A., Busto, P., Marshak-Rothstein, A., Ksander, B. R., & Gregory-Ksander, M. (2016). Overexpression of Soluble Fas Ligand following Adeno-Associated Virus Gene Therapy Prevents Retinal Ganglion Cell Death in Chronic and Acute Murine Models of Glaucoma. *J Immunol*, *197*(12), 4626-4638. doi:10.4049/jimmunol.1601488
- Krizaj, D. (1995). What is glaucoma? In H. Kolb, E. Fernandez, & R. Nelson (Eds.), *Webvision: The Organization of the Retina and Visual System*. Salt Lake City (UT): University of Utah Health Sciences Center
- Leppert, C. A., Diekmann, H., Paul, C., Laessing, U., Marx, M., Bastmeyer, M., & Stuermer, C. A. (1999). Neurolin Ig domain 2 participates in retinal axon guidance and Ig domains 1 and 3 in fasciculation. *J Cell Biol*, *144*(2), 339-349.
- Li, C., & Chan, Y. R. (2011). Lipocalin 2 regulation and its complex role in inflammation and cancer. *Cytokine*, *56*(2), 435-441. doi:10.1016/j.cyto.2011.07.021
- Li, S., Cai, J., Feng, Z. B., Jin, Z. R., Liu, B. H., Zhao, H. Y., . . . Xing, G. G. (2017). BDNF Contributes to Spinal Long-Term Potentiation and Mechanical Hypersensitivity Via Fyn-Mediated Phosphorylation of NMDA Receptor GluN2B Subunit at Tyrosine 1472 in Rats Following Spinal Nerve Ligation. *Neurochem Res*, *42*(10), 2712-2729. doi:10.1007/s11064-017-2274-0
- Libby, R. T., Anderson, M. G., Pang, I. H., Robinson, Z. H., Savinova, O. V., Cosma, I. M., . . . John, S. W. (2005). Inherited glaucoma in DBA/2J mice: pertinent disease features for studying the neurodegeneration. *Vis Neurosci*, *22*(5), 637-648. doi:10.1017/S0952523805225130
- Liddelow, S. A., Guttenplan, K. A., Clarke, L. E., Bennett, F. C., Bohlen, C. J., Schirmer, L., . . . Barres, B. A. (2017). Neurotoxic reactive astrocytes are induced by activated microglia. *Nature*, *541*(7638), 481-487. doi:10.1038/nature21029
- Mantravadi, A. V., & Vadhar, N. (2015). Glaucoma. *Prim Care*, *42*(3), 437-449. doi:10.1016/j.pop.2015.05.008
- Nakazawa, T., Nakazawa, C., Matsubara, A., Noda, K., Hisatomi, T., She, H., . . . Benowitz, L. I. (2006). Tumor necrosis factor-alpha mediates oligodendrocyte death and delayed retinal ganglion cell loss in a mouse model of glaucoma. *J Neurosci*, *26*(49), 12633-12641. doi:10.1523/JNEUROSCI.2801-06.2006
- Pekny, M., & Pekna, M. (2014). Astrocyte reactivity and reactive astrogliosis: costs and benefits. *Physiol Rev*, *94*(4), 1077-1098. doi:10.1152/physrev.00041.2013

- Qu, J., & Jakobs, T. C. (2013). The Time Course of Gene Expression during Reactive Gliosis in the Optic Nerve. *PLoS One*, 8(6), e67094. doi:10.1371/journal.pone.0067094
- Quigley, H. A. (2011). Glaucoma. *Lancet*, 377(9774), 1367-1377. doi:S0140-6736(10)61423-7 [pii]
- Roh, M., Zhang, Y., Murakami, Y., Thanos, A., Lee, S. C., Vavvas, D. G., . . . Miller, J. W. (2012). Etanercept, a widely used inhibitor of tumor necrosis factor-alpha (TNF-alpha), prevents retinal ganglion cell loss in a rat model of glaucoma. *PLoS One*, 7(7), e40065. doi:10.1371/journal.pone.0040065
- Rovere, G., Nadal-Nicolas, F. M., Sobrado-Calvo, P., Garcia-Bernal, D., Villegas-Perez, M. P., Vidal-Sanz, M., & Agudo-Barriuso, M. (2016). Topical Treatment With Bromfenac Reduces Retinal Gliosis and Inflammation After Optic Nerve Crush. *Invest Ophthalmol Vis Sci*, 57(14), 6098-6106. doi:10.1167/iovs.16-20425
- Sappington, R. M., Carlson, B. J., Crish, S. D., & Calkins, D. J. (2010). The microbead occlusion model: a paradigm for induced ocular hypertension in rats and mice. *Invest Ophthalmol Vis Sci*, 51(1), 207-216. doi:iovs.09-3947 [pii]
- Schehlein, E. M., & Robin, A. L. (2019). Rho-Associated Kinase Inhibitors: Evolving Strategies in Glaucoma Treatment. *Drugs*, 79(10), 1031-1036. doi:10.1007/s40265-019-01130-z
- Shabab, T., Khanabdali, R., Moghadamtousi, S. Z., Kadir, H. A., & Mohan, G. (2017). Neuroinflammation pathways: a general review. *Int J Neurosci*, 127(7), 624-633. doi:10.1080/00207454.2016.1212854
- Sofroniew, M. V. (2014). Astrogliosis. *Cold Spring Harb Perspect Biol*, 7(2), a020420. doi:10.1101/cshperspect.a020420
- Song, J., & Kim, O. Y. (2018). Perspectives in Lipocalin-2: Emerging Biomarker for Medical Diagnosis and Prognosis for Alzheimer's Disease. *Clin Nutr Res*, 7(1), 1-10. doi:10.7762/cnr.2018.7.1.1
- Soto, I., & Howell, G. R. (2014). The complex role of neuroinflammation in glaucoma. *Cold Spring Harb Perspect Med*, 4(8). doi:10.1101/cshperspect.a017269
- Spandidos, A., Wang, X., Wang, H., & Seed, B. (2010). PrimerBank: a resource of human and mouse PCR primer pairs for gene expression detection and quantification. *Nucleic Acids Res*, 38(Database issue), D792-799. doi:10.1093/nar/gkp1005
- Sun, D., Lye-Barthel, M., Masland, R. H., & Jakobs, T. C. (2009). The morphology and spatial arrangement of astrocytes in the optic nerve head of the mouse. *J Comp Neurol*, 516(1), 1-19. doi:10.1002/cne.22058

- Sun, D., Lye-Barthel, M., Masland, R. H., & Jakobs, T. C. (2010). Structural remodeling of fibrous astrocytes after axonal injury. *J Neurosci*, *30*(42), 14008-14019. doi:10.1523/JNEUROSCI.3605-10.2010
- Sun, D., Moore, S., & Jakobs, T. C. (2017). Optic nerve astrocyte reactivity protects function in experimental glaucoma and other nerve injuries. *J Exp Med*, *214*(5), 1411-1430. doi:10.1084/jem.20160412
- Sun, D., Qu, J., & Jakobs, T. C. (2013). Reversible reactivity by optic nerve astrocytes. *Glia*, *61*(8), 1218-1235. doi:10.1002/glia.22507
- Tamcelik, N., Atalay, E., Cicik, E., & Ozkok, A. (2015). Comparability of Icare Pro Rebound Tonometer with Goldmann Applanation and Noncontact Tonometer in a Wide Range of Intraocular Pressure and Central Corneal Thickness. *Ophthalmic Res*, *54*(1), 18-25. doi:10.1159/000381781
- Tham, Y. C., Li, X., Wong, T. Y., Quigley, H. A., Aung, T., & Cheng, C. Y. (2014). Global prevalence of glaucoma and projections of glaucoma burden through 2040: a systematic review and meta-analysis. *Ophthalmology*, *121*(11), 2081-2090. doi:10.1016/j.ophtha.2014.05.013
- Wang, R., Seifert, P., & Jakobs, T. C. (2017). Astrocytes in the Optic Nerve Head of Glaucomatous Mice Display a Characteristic Reactive Phenotype. *Invest Ophthalmol Vis Sci*, *58*(2), 924-932. doi:10.1167/iovs.16-20571
- Xing, C., Wang, X., Cheng, C., Montaner, J., Mandeville, E., Leung, W., . . . Lo, E. H. (2014). Neuronal production of lipocalin-2 as a help-me signal for glial activation. *Stroke*, *45*(7), 2085-2092. doi:10.1161/STROKEAHA.114.005733
- Yang, C. F., Lin, S. P., Chiang, C. P., Wu, Y. H., H'Ng W, S., Chang, C. P., . . . Wu, J. Y. (2018). Loss of GPNMB Causes Autosomal-Recessive Amyloidosis Cutis Dyschromica in Humans. *Am J Hum Genet*, *102*(2), 219-232. doi:10.1016/j.ajhg.2017.12.012
- Zamanian, J. L., Xu, L., Foo, L. C., Nouri, N., Zhou, L., Giffard, R. G., & Barres, B. A. (2012). Genomic analysis of reactive astrogliosis. *J Neurosci*, *32*(18), 6391-6410. doi:10.1523/JNEUROSCI.3605-10.2010 [pii]